Precision and Accuracy Measurement of a Leaf Spring Arm for Mobile Robots

Yun-Ju Chuang [1,*], Qinxin Zhan [2], Ho Chang [3,4], Yin-Tung Sun [1], and Tsing-Tshih Tsung [1]

[1] Department of Mechanical Engineering, Minghsin University of Science and Technology (MUST), Taiwan
[2] College of Mechanical and Electrical Engineering, National Taipei University of Technology (NTUT), Taiwan
[3] Ph.D Program in Semiconductor Technology, Minghsin University of Science and Technology (MUST), Taiwan
[4] Innovation Frontier Institute of Research for Science and Technology,
National Taipei University of Technology (NTUT), Taiwan
Email: andy2551468@gmail.com (Y.-J.C.); q364849548@gmail.com (Q.Z.); hchang@must.edu.tw (H.C.);
ytasun@must.edu.tw (Y.-T.S.); tttsung@gmail.com (T.-T.T.)
*Corresponding author

***Abstract*—This paper presents the design and experimental characterization of a leaf-spring mechanism developed as an extensible arm for mobile robotic platforms. The mechanism uses two oppositely oriented curved steel strips as its deployable element and uses a timing-belt transmission for extension and retraction. Two complementary experiments were conducted: a static-deformation test, which covered applied tip loads of 0–5 N and extension lengths of 100–600 mm, and ae positioning-repeatability test, which covered loads of 0–3 N and extension lengths of 100–500 mm. Static deformation was determined from arm-tip height differences, while positioning repeatability was evaluated from repeated laser-spot markings on a target plane. Ten trials were performed for each tested condition. The results showed that static deformation increased with extension length and generally increased with applied load. The dispersion of the laser-spot markings also tended to increase at longer extensions. These findings characterize the load- and extension-dependent behavior of the proposed mechanism and provide an experimental basis for the subsequent refinement of long-stroke compliant robotic arms.**

***Keywords*—leaf-spring mechanism, extensible arm, static deformation, positioning repeatability, mobile robotic platforms**

I. Introduction

In precision engineering, compliant and flexible mechanisms have received significant attention because of their inherent advantages over conventional rigid-body joints. They offer several benefits including reduced backlash, simplified assembly, and high-resolution motion transmission [1, 2]. These mechanisms exploit elastic deformation to achieve the desired kinematic functions, and their designs have been systematically explored using analytical models and computational optimization techniques [3]. Among the available configurations, leaf-spring-based structures offer a balanced compromise among deployability, structural simplicity, and manufacturing feasibility [4, 5]. Nevertheless, the compliance that enables motion introduces challenges in achieving high precision and accurate positioning, particularly under varying loads and extended stroke ranges.

Accurate characterization of stiffness and deformation behavior is critical for predicting the performance of compliant mechanisms. Several methodologies for stiffness identification and modeling have been developed, including the identification of elastostatic parameters via Computer-Aided Design (CAD)-embedded virtual experiments [6] and the use of lumped-parameter stiffness models for complex manipulator links [7]. Recent studies have also established formal links between measurement theory and the evaluation of the accuracy and precision of compliant systems, proposing statistical frameworks to quantify these qualities [8]. Concurrently, precision flexure-based mechanisms, such as hexapods and micrograppers, have been designed and experimentally validated, highlighting the importance of stiffness optimization for improved repeatability and load capacity [9, 10].

Despite these advances, most existing studies have focused on multi-degree-of-freedom flexure systems or micromanipulation devices, and few have experimentally characterized the effects of applied load and extension length on large-stroke extensible compliant arms. To address this gap, a leaf-spring extensible mechanism was proposed in this study and its static deformation and positioning repeatability were evaluated through two complementary experiments. The static deformation test covered applied tip loads of 0–5 N and extension lengths of 100–600 mm, whereas the positioning-repeatability test covered applied tip loads of 0–3 N and extension lengths of 100–500 mm. Static deformation was determined from arm tip height differences, and positioning repeatability was evaluated using repeated laser spot markings on a

Manuscript received May 19, 2026; revised June 15, 2026; accepted August 19, 2026; published November 20, 2026.

target plane. This experimental framework provides quantitative static deformation data and qualitative observations of positioning repeatability under different load and extension conditions.

II. Related Work

A. Compliant and Leaf-Spring Mechanism Design

Compliant mechanisms leverage elastic deformation to replace rigid-body joints, providing backlash-free motion, enhanced reliability, and simplified assembly [1, 11]. The seminal work of Howell *et al.* [12] established systematic design methodologies for compliant flexure elements, including pseudo-rigid-body models and parametric synthesis techniques. Optimization-based design methods that combine finite element analysis with metaheuristic algorithms have also been developed for compliant mechanisms [13].

Leaf springs are a prevalent class of compliant elements due to their relative simplicity and ease of integration into deployable systems. Analytical studies have derived closed-form stiffness models for leaf-spring systems under bending and combined loading conditions, expanding the design space for stiffness-tailored applications [14]. Parallel-compliant platforms incorporating leaf-spring linkages have been proposed to achieve large workspace coverage with constrained compliance [15]. Recent research has extended compliant design to include optimized leaf-spring geometries based on topology optimization and energy-based performance metrics [16].

Design innovations have further integrated compliant leaf structures into multifunctional mechanisms, including compliant grippers [17], compliant joints with decoupled motion axes [18], and modular flexure interfaces for robotic manipulators [19]. However, most existing design work focuses on small stroke ranges or predefined motion pathways, with limited investigation of extensible leaf-spring configurations for large stroke and load variations—a gap addressed in this study.

B. Precision Measurement and Positioning Performance

Accurate quantification of precision and accuracy is fundamental for evaluating compliant mechanisms, particularly in the context of elastic deformation. Precision is commonly quantified through statistical variations in repeated measurements, whereas accuracy is expressed as the deviation from a reference target [2]. Laser displacement sensors have been extensively used to achieve submicron resolutions in compliant motion measurements, complementing optical encoders and interferometric systems [20]. Coordinate measuring machines and vision-based tracking methods have been shown to enhance the spatial measurement capabilities of flexible structures [21, 22].

Metrics such as root-mean-square error, standard deviation, and systematic bias offer insights into both repeatability and accuracy. However, interpreting these metrics in compliant systems requires carefully decoupling elastic effects, measurement noise, and geometric nonlinearities [23, 24]. Campanile and Hasse [25] proposed a refined conceptual framework that distinguishes intrinsic compliant mechanism errors from measurement system variability, highlighting the need for robust analytical and experimental design strategies.

In addition to measurement techniques, recent studies have emphasized experimental design and statistical methods for evaluating systematic deformation under load. Replicated experiments combined with regression models have been used to identify and isolate error sources such as gravity-induced deflection, hysteresis, and thermal drift [26]. These frameworks establish the theoretical foundation for the integrated measurement approach used in this research, which aims to quantify the performance of leaf spring arms under varying stroke and load conditions.

C. Structural Stiffness Modeling and Performance Optimization

Stiffness is a pivotal factor in the performance of compliant mechanisms, influencing both static positioning error and dynamic response. Early stiffness modeling approaches adopted lumped compliance matrices to approximate elastic behavior, enabling analytical tractability in design iterations [27, 28]. Finite Element Analysis (FEA) remains a standard for high-fidelity evaluation of compliant elements, accurately capturing stress distributions and deformation patterns under complex loading [29]. A combination of analytical models and FEA calibration has been shown to achieve a balance between accuracy and computational efficiency [30].

A study on the gravitational effects on elongated compliant structures has demonstrated that the orientation of these structures relative to gravity significantly alters both the deflection profiles and positioning stability [31]. Several techniques have been developed to compensate for or mitigate gravity induced errors. These include preloaded constraint designs, counterbalance elements, and stiffness enhancements through geometric reinforcement [32–34]. The objectives of these modifications are twofold: first, to reduce displacement variation, and second, to minimize systematic drift without compromising compliance benefits.

Optimization methodologies for compliant mechanisms incorporate multi-objective criteria and balance stiffness, mass, and workspace requirements using global search and gradient-based algorithms [35, 36]. These studies emphasize the inherent tradeoffs in compliant design, particularly between flexibility and precision, and highlight the need for experimentally validated stiffness strategies that can guide practical mechanism development. This research builds on these insights by correlating structural stiffness characteristics with precision and accuracy outcomes for leaf-spring extensible arms under realistic loading scenarios.

III. Methodology

A. Mechanical Structure of the Leaf-Spring Robotic Arm

The proposed robotic arm uses an extensible leaf-spring structure as its primary load-bearing element. The mechanism consists of three main subsystems: the leaf-spring arm, a belt-driven transmission system, and an aluminum support frame, as shown in Fig. 1(a) and (b). The timing belt (Fig. 1(d)) and pulley (Fig. 1(e)) system drives the linear extension and retraction of the leaf-spring

arm. The leaf-spring arm has a curved cross-sectional profile with a central arc angle of approximately 86°, a width of 32 mm, and a thickness of 0.13 mm, as shown in Fig. 1(c). The curved cross-section was selected to increase out-of-plane stiffness while retaining elastic compliance. The arm was mounted on the aluminum support frame in a cantilever configuration and provides a nominal extension range of 0–600 mm.

The toothed belt segment was attached along the upper steel strip of the leaf-spring arm, as shown in Fig. 2, so that its teeth could engage with the timing pulley during extension and retraction. Two oppositely oriented steel strips were joined using cloth-backed adhesive tape.

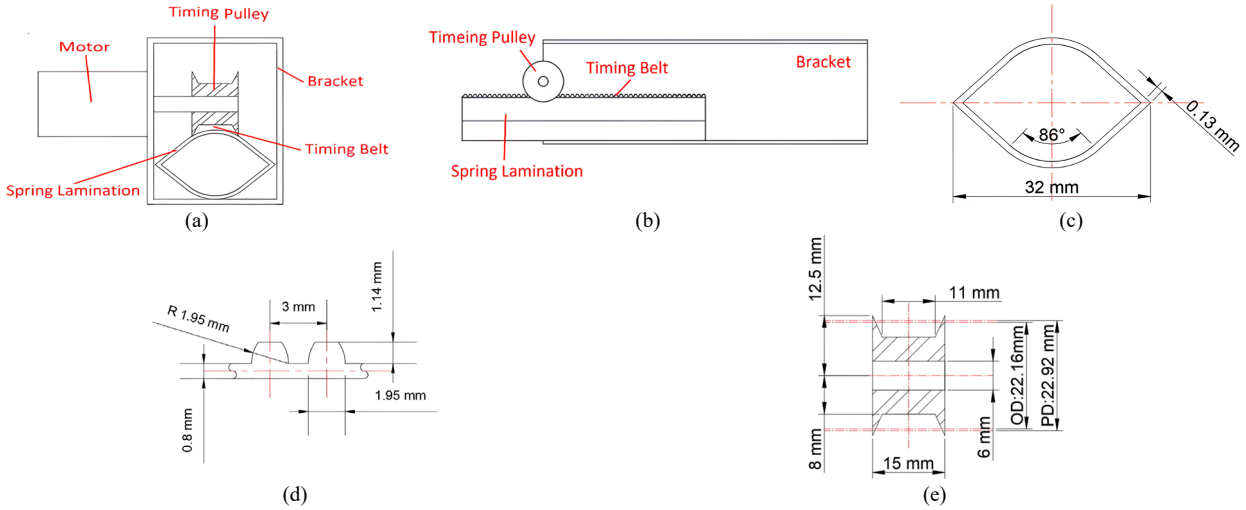


Fig. 1. Mechanical configuration and component dimensions of the leaf-spring arm: (a) front view; (b) side view; (c) cross-sectional dimensions of the curved steel strip; (d) cross-sectional dimensions of the timing belt; and (e) dimensions of the timing pulley.

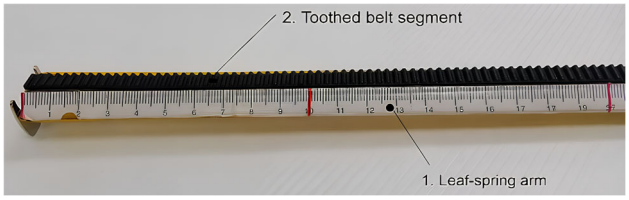
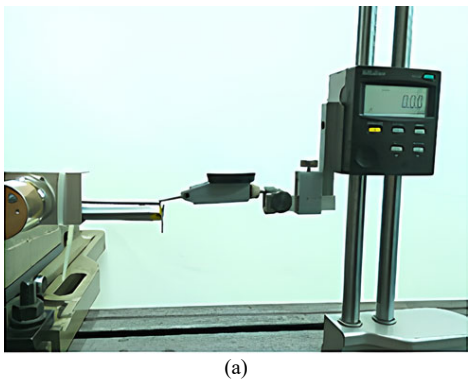


Fig. 2 Physical configuration of the leaf-spring arm and the toothed belt segment.

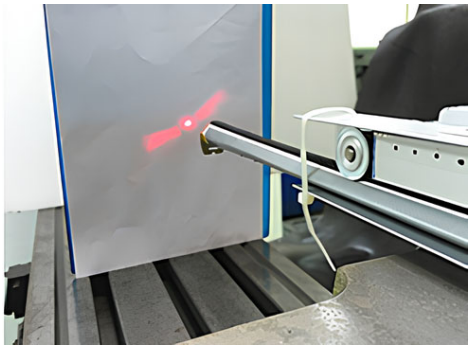
B. Experimental Setup

Experiments were conducted to evaluate the static deformation and positioning repeatability of the leaf-spring arm under prescribed load and extension conditions. The experimental platform consisted of a rigid aluminum frame, a DC motor-driven timing-belt mechanism, the leaf-spring arm, and the associated measurement devices.

The experimental setups used to measure static deformation and positioning repeatability are shown in Fig. 3(a) and (b), respectively.



(a)



(b)

Fig. 3. Experimental arrangements used in this study: (a) digital height-gauge setup for the static-deformation test conducted at 0–5 N and 100–600 mm; (b) laser-pointer-and-target setup for the positioning-repeatability test conducted at 0–3 N and 100–500 mm.

The leaf-spring arm was mounted on a rigid aluminum frame. Extension and retraction were driven by a timing belt and pulley mechanism using a 12 V, 100 mA, 6,000 rpm DC motor. The extension and retraction directions were controlled manually using a remote controller. A commercially available red laser pointer was mounted on the tip of the leaf-spring arm, and a plain white paper target was positioned 50 mm from the arm tip, as shown in Fig. 3(b). The manufacturer, model, and wavelength of the laser pointers were not recorded. The laser pointer was used only as an optical position marker, not as a calibrated displacement sensor. For each prescribed extension and load condition, the arm was stopped, and the measurement was taken only after no visible oscillation was observed; no fixed settling time was imposed. The center of the laser spot was manually marked on the target with a pen. Each condition was repeated ten

times. The straight-line distance between each marked point and the reference point was measured with a digital caliper with a resolution of 0.01 mm. The target paper contained no printed scale, and no image-based coordinate extraction procedure was used.

The two tests used different loads and extension ranges. The digital height gauge test applied tip loads from 0 to 5 N in 1 N increments, and extension lengths from 100 to 600 mm in 100 mm increments. The laser pointer-and-target test applied tip loads from 0 to 3 N in 1 N increments, and extension lengths from 100 to 500 mm in 100 mm increments. The fully retracted position at 0 mm was used as the reference in both tests, and ten repeated trials were performed for each test condition. In the static deformation test, a condition was classified as overload if the arm could not support the applied load or reach the prescribed extension, and no numerical result was assigned to that condition.

C. Experimental Procedure

The experimental procedure consisted of two complementary tests: a static deformation test using a digital height gauge, and a positioning-repeatability test using a laser pointer and a target plane, as shown in Fig. 3(a) and (b), respectively. The static deformation test covered applied tip loads of 0–5 N and extension lengths of 100–600 mm, whereas the positioning-repeatability test covered applied tip loads of 0–3 N and extension lengths of 100–500 mm. In both tests, the fully retracted 0 mm position was used as the reference, and ten independent retract-and-extend trials were conducted for each test condition. The detailed procedures for the two tests are described below.

For each static deformation trial, the arm was first returned to the fully retracted 0 mm position and then extended to the prescribed length under the specified tip load. After no visible oscillations were observed, the vertical position of the arm tip was measured using a digital height gauge, and no fixed settling time was imposed. The static deformation was determined from the height difference between the measured arm tip position and the reference position.

As a simplified theoretical reference, the extended arm may be idealized as an Euler–Bernoulli cantilever beam subjected to a transverse tip load. Assuming small deformation, the bending moment–curvature relationship is expressed as follows:

$$EI\frac{d^2y(x)}{dx^2} = M(x) \tag{1}$$

where E is Young's modulus,I is the second moment of area of the beam cross-section, $y(x)$ is the transverse deflection, and $M(x)$ is the bending moment at position x. For an ideal uniform cantilever of length L subjected to a concentrated tip load F, integrating Eq. (1) with the fixed-end boundary conditions gives the theoretical tip deflection:

$$\delta_{beam} = \frac{FL^3}{3EI} \tag{2}$$

The corresponding idealized cantilever stiffness is:

$$k_{beam} = \frac{F}{\delta_{beam}} = \frac{3EI}{L^3} \tag{3}$$

Eqs. (2) and (3) indicate that the deformation of an ideal cantilever increases with an extended cube length, whereas its stiffness decreases. However, these equations only describe the expected qualitative length dependence. The proposed arm consists of two initially thin curved steel strips connected to a timing belt and joined using cloth-backed adhesive tape. Therefore, it may exhibit cross-sectional deformation, contact effects, geometric nonlinearity, and self-weight deformation, which are not represented by an ideal straight beam model. Consequently, these equations were not used to calculate the effective stiffness or to quantitatively predict the measured deformation in this study.

For a given applied load F and extension length L, the mean static deformation was calculated as follows:

$$\bar{\delta}(F,L) = \frac{1}{n}\sum_{i=1}^{n}\delta_i(F,L) \tag{4}$$

where $\delta_i(F,L)$ is the static deformation measured in the $i\text{-}th$ trial and $n = 10$. The corresponding standard deviations of the samples were calculated as follows:

$$s_\delta(F,L) = \sqrt{\frac{\sum_{i=1}^{n}\left[\delta_i(F,L)-\bar{\delta}(F,L)\right]^2}{n-1}} \tag{5}$$

A positioning repeatability test was conducted under applied loads ranging from 0 to 3 N and extension lengths ranging from 100 to 500 mm in 100 mm increments. A red laser pointer was mounted on the arm tip, and a plain white paper target was positioned 50 mm from the tip. The laser spot obtained at the fully retracted position was used as the reference point. For each trial, the arm was first returned to the fully retracted position and then extended to the prescribed length under the specified tip load. After visible oscillation ceased, the center of the laser spot was manually marked on the target with a pen, and no fixed settling time was imposed. This retract-and-extend procedure was repeated ten times for each tested condition. The straight-line distance between each marked point and the reference point was measured with a digital caliper with a resolution of 0.01 mm. The resulting laser spot distributions and measured error ranges were used to evaluate positioning repeatability.

IV. Results and Discussion

A. Static Deformation of the Leaf-Spring Arm

Table I summarizes the mean static deformation and sample standard deviation obtained from ten repeated measurements for each feasible load–extension condition, while Fig. 4 plots the corresponding mean values. For every feasible load condition, the mean static deformation increased with extension length. Under the 0 N condition, the mean static deformation increased from 0.066 mm at an extension length of 100 mm to 14.794 mm at 600 mm.

At an extension length of 400 mm, the mean static deformation increased from 3.416 mm at 0 N to 52.189 mm at 5 N. These results demonstrate that both the extension length and the applied tip load influenced the measured static deformation.

The effect of the applied load was more pronounced at longer extension lengths. At 300 mm, the mean static deformation ranged from 1.645 mm at 0 N to 23.023 mm at 5 N. Numerical results were obtained at 500 mm under loads of 0–3 N, with mean deformation values of 10.638, 27.609, 47.698, and 59.042 mm. The 4 and 5 N conditions at 500 mm were classified as overloads. At 600 mm, numerical results were obtained only under loads of 0, 1, and 2 N, whereas the 3–5 N conditions were classified as overloads. No numerical statistics were calculated for overload conditions.

TABLE I. MEAN STATIC DEFORMATION OF THE LEAF-SPRING ARM UNDER DIFFERENT LOAD AND EXTENSION CONDITIONS

Extension length (mm)	0 N	1 N	2 N	3 N	4 N	5 N
100	0.066±0.023	0.884±0.053	1.694±0.352	1.277±0.191	2.344±0.431	2.481±0.263
200	0.377±0.018	1.935±0.489	5.615±0.389	5.231±0.246	7.618±0.415	9.100±0.626
300	1.645±0.053	6.864±2.140	12.410±0.175	14.243±0.742	18.671±0.560	23.023±0.523
400	3.416±0.049	14.481±0.493	24.792±0.350	28.472±0.499	39.575±1.001	52.189±0.689
500	10.638±0.827	27.609±0.598	47.698±1.103	59.042±1.654	Overload	Overload
600	14.794±1.107	45.207±0.914	87.387±0.643	Overload	Overload	Overload

Note: Values are reported as mean ± sample standard deviation in millimeters based on ten repeated measurements for each feasible condition. Conditions at which the arm could not support the prescribed load or reach the specified extension were classified as overload, and no numerical statistics were calculated.

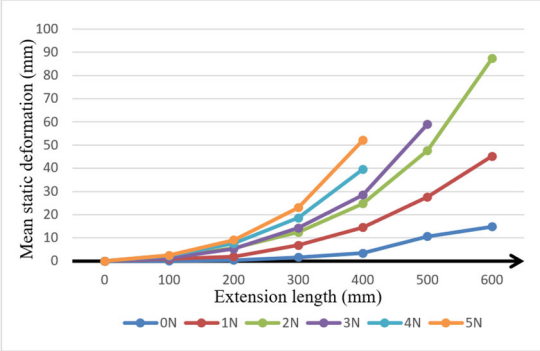


Fig. 4. Mean static deformation of the leaf-spring arm as a function of extension length under applied tip loads of 0–5 N. Conditions at which the arm could not support the prescribed load or reach the specified extension were classified as overload and are not plotted as numerical values.

Overall, the measured static deformation increased with the extension length under every feasible load condition, and the magnitude of the deformation generally increased with the applied load. The occurrence of overloads at longer extensions and higher loads indicated that the feasible load range decreased as the arm was extended. The observed increase in deformation with extension length is qualitatively consistent with the length-dependent trend indicated by the ideal cantilever-beam relation in Eq. (2). However, no quantitative theoretical–experimental comparison or finite element analysis has been performed, because the initially curved coupled-strip structure does not satisfy the assumptions of an ideal uniform straight cantilever beam.

B. Laser-Spot Distribution Results

The positioning repeatability test was conducted under applied tip loads of 0–3 N and extension lengths of 100–500 mm in 100 mm increments. Ten repeated retract-and-extend trials were performed for each load–extension condition. In every trial, the arm was first fully retracted to the 0 mm reference position and then extended to the prescribed length. After visible oscillations ceased, the center of the laser spot was manually marked on the target paper. The distributions of the ten marked points under each condition are shown in Figs. 5–8. Because no image-based coordinate extraction procedure was used, these figures were interpreted qualitatively in terms of the observed positional variation rather than through a quantitative, coordinate-based analysis.

1) 0 N load condition

Under the 0 N load condition, the laser spot distributions from ten repeated trials are shown in Fig. 5. The marked points remained distributed around the reference point for all tested extension lengths. Differences in the spread and location of the marked points were observed among the five extension conditions. In particular, the distributions at 400 and 500 mm appeared more dispersed than those at shorter extensions. Because image-based coordinate extraction was not performed, these distributions were interpreted qualitatively, and no numerical comparison of repeatability among the extension lengths was made.

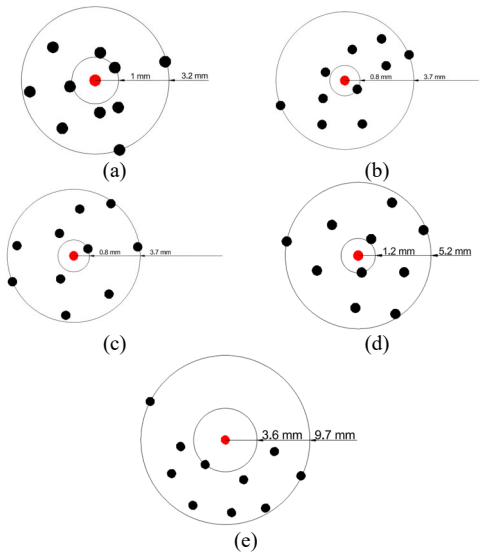


Fig. 5. Laser-spot distributions obtained from ten repeated trials at extension lengths of (a) 100 mm, (b) 200 mm, (c) 300 mm, (d) 400 mm, and (e) 500 mm under the 0 N load condition. The red point denotes the reference position obtained with the arm fully retracted.

2) 1 N load condition

Under the 1 N load condition, the laser spot distributions from ten repeated trials are shown in Fig. 6. Differences in the spread and location of the marked points were observed among the tested extension lengths. Distributions at longer extensions generally covered a larger area than those at shorter extensions, indicating greater positional variation in repeated trials. Because the spot coordinates were not extracted using an image-based method, no quantitative comparison was made with the 0 N condition.

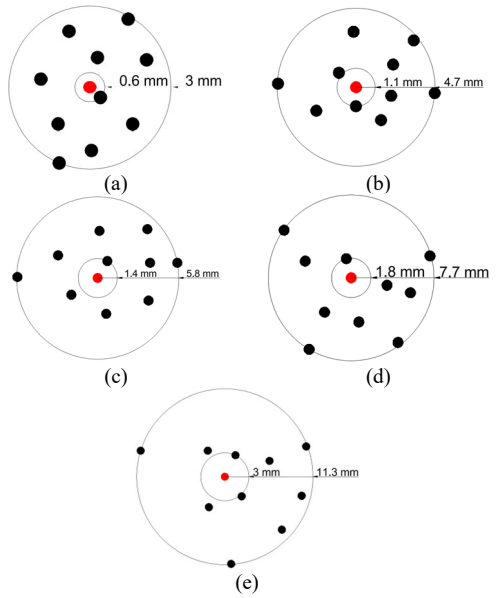


Fig. 6. Laser-spot distributions obtained from ten repeated trials at extension lengths of (a) 100 mm, (b) 200 mm, (c) 300 mm, (d) 400 mm, and (e) 500 mm under the 1 N load condition. The red point denotes the reference position with the arm fully retracted.

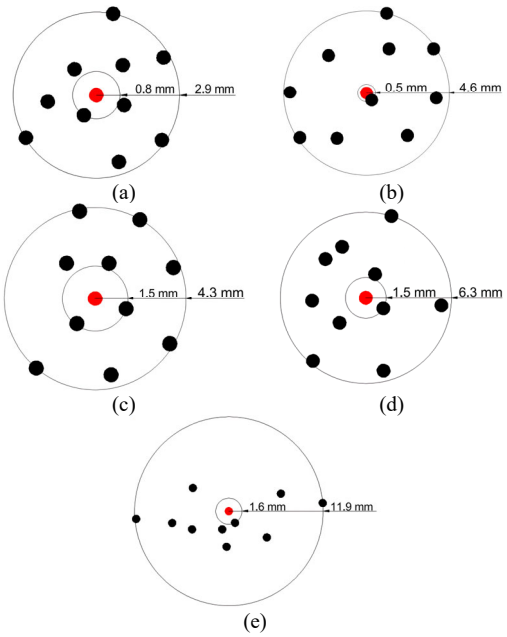


Fig. 7. Laser-spot distributions obtained from ten repeated trials at extension lengths of (a) 100 mm, (b) 200 mm, (c) 300 mm, (d) 400 mm, and (e) 500 mm under the 2 N load condition. The red point denotes the reference position with the arm fully retracted.

3) 2 N load condition

Under the 2 N load condition, the laser spot distributions obtained from ten repeated trials are shown in Fig. 7. Differences in the spread and location of the marked points were observed among the tested extension lengths. At an extension length of 400 mm, the marked points appeared displaced toward one side of the reference point, indicating a directional positional variation across the repeated trials. Because vibration and torsional deformation were not measured independently, the cause of the observed distribution could not be determined from the present experiment.

4) 3 N load condition

Under the 3 N load condition, the laser spot distributions obtained from ten repeated trials are shown in Fig. 8. Differences in the spread and location of the marked points were observed between the tested extension lengths. The distributions at longer extensions appeared more dispersed than those at shorter extensions, indicating greater positional variation among the repeated trials. Because the experiment did not independently measure the bending moment, structural deformation, or vibration, the observed distributions could not be attributed to specific mechanical causes.

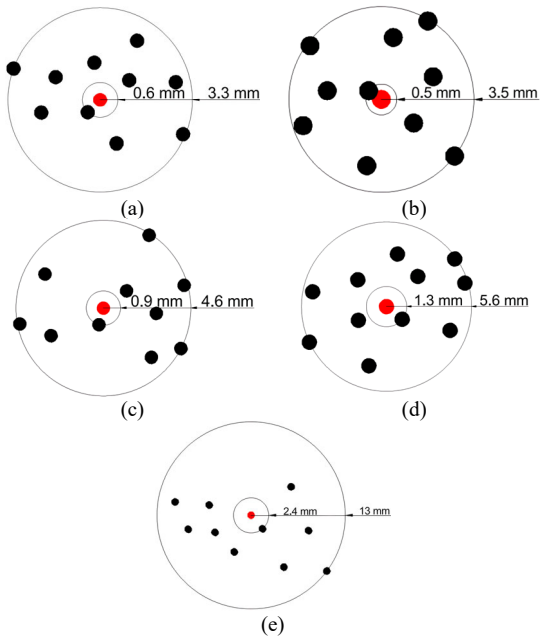


Fig. 8. Laser-spot distributions obtained from ten repeated trials at extension lengths of (a) 100 mm, (b) 200 mm, (c) 300 mm, (d) 400 mm, and (e) 500 mm under the 3 N load condition. The red point denotes the reference position with the arm fully retracted.

V. Conclusion

This paper presents the design and experimental evaluation of a leaf-spring extensible arm driven by a timing belt mechanism. Two complementary experiments were conducted. The static deformation test covered applied tip loads of 0–5 N and extension lengths of 100–600 mm, whereas the positioning repeatability test covered applied tip loads of 0–3 N and extension lengths

of 100–500 mm. Ten repeated trials were conducted for each test condition.

The static deformation results showed that mean deformation increased with extension length at every feasible load condition and generally increased with applied load. Overload occurred at longer extensions under higher loads, indicating that the feasible load range decreased as the arm was extended. The laser spot distributions differed between the test load and extension conditions. Greater positional variation was generally observed at longer extensions; however, these distributions were interpreted qualitatively because no image-based coordinate extraction procedures were used.

These results characterize the deformation and positioning repeatability behavior of the proposed leaf-spring arm under the tested operating conditions. These findings provide experimental information for evaluating the applicability of this extensible mechanism to mobile robotic platforms. Further quantitative investigation of laser spot distributions is required to establish numerical positioning performance metrics and to determine the mechanical causes of the observed positional variation.

CONFLICT OF INTEREST

The authors declare no conflict of interest.

AUTHOR CONTRIBUTIONS

Y.-J.C. conceived and designed the experiments, performed the primary writing of the manuscript, and revised it for important intellectual content; Q.Z. was responsible for robot fabrication, data collection, sample analysis, and figure preparation; H.C. provided research advice and expertise; Y.-T.S. assisted in English editing and text refinement; T.-T.T. provided recommendations for mechanism fabrication. All authors have approved the final version.

REFERENCES

[1] L. L. Howell, "Compliant mechanisms," in *Proc. 21st Century kinematics: The 2012 NSF Workshop*, Springer, pp. 189–216, 2013. doi: 10.1007/978-1-4471-4510-3

[2] L. F. Campanile, S. Kirmse, and A. Hasse, "Accuracy and precision: A new view on kinematic assessment of solid-state hinges and compliant mechanisms," *Journal of Intelligent Material Systems and Structures,* vol. 33, no. 13, pp. 1743–1748, 2022. doi: 10.1177/1045389X211064323

[3] M. Kabganian and S. M. Hashemi, "Towards design optimization of compliant mechanisms: A hybrid pseudo-rigid-body model–finite element method approach and an accurate empirical compliance equation for circular flexure hinges," *Biomimetics,* vol. 9, no. 8, 471, 2024. doi: 10.3390/biomimetics9080471

[4] K. Feng *et al.*, "Design and modeling of a two-axis compliant joint based on flexure leaf springs," *Machines,* vol. 14, no. 3, 313, 2026. doi: 10.3390/machines14030313

[5] J. P. Meijaard, D. M. Brouwer, and J. B. Jonker, "Analytical and experimental investigation of a parallel leaf spring guidance," *Multibody System Dynamics,* vol. 23, no. 1, pp. 77–97, 2010. doi: 10.1007/s11044-009-9172-4

[6] A. Klimchik, A. Pashkevich, and D. Chablat, "CAD-based approach for identification of elasto-static parameters of robotic manipulators," *Finite Elements in Analysis and Design,* vol. 75, pp. 19–30, 2013. doi: 10.1016/j.finel.2013.06.008

[7] A. Pashkevich, A. Klimchik, D. Chablat, and P. Wenger, "Accuracy improvement for stiffness modeling of parallel manipulators," arXiv preprint, arXiv:0909.1460, 2009.

[8] F. Santoni, A. De Angelis, I. Skog, A. Moschitta, and P. Carbone, "Calibration and characterization of a magnetic positioning system using a robotic arm," *IEEE Transactions on Instrumentation and Measurement,* vol. 68, no. 5, pp. 1494–1502, 2018. doi: 10.1109/TIM.2018.2885590

[9] M. Naves, M. Nijenhuis, B. Seinhorst, W. Hakvoort, and D. M. Brouwer, "T-Flex: A fully flexure-based large range of motion precision hexapod," *Precision engineering,* vol. 72, pp. 912–928, 2021. doi: 10.1016/j.precisioneng.2021.08.015

[10] A. P. Doroliat, T.-Y. Ku, and C.-H. G. Li, "Innovative grasping system with versatility and automation," *The International Journal of Advanced Manufacturing Technology,* vol. 126, no. 11, pp. 5339–5352, 2023. doi: 10.1007/s00170-023-11398-x

[11] S. T. Smith, *Flexures: Elements of Elastic Mechanisms*, CRC Press, 2000. doi: 10.1201/9781482282962

[12] L. L. Howell and A. Midha, "A method for the design of compliant mechanisms with small-length flexural pivots," *Journal of Mechanical Design,* vol. 116, no. 1, pp. 280–290, 1994. doi: 10.1115/1.2919359

[13] N. Le Chau, N. T. Tran, and T.-P. Dao, "An optimal design method for compliant mechanisms," *Mathematical Problems in Engineering,* vol. 2021, no. 1, 5599624, 2021. doi: 10.1155/2021/5599624

[14] P. Li, Z.-R. Tong, and W.-H. Zhang, "Analytical model establishment and attitude calculation of a parallel leaf-spring carrying mechanism," *Mechanical Sciences,* vol. 13, no. 1, pp. 311–320, 2022. doi: 10.5194/ms-13-311-2022

[15] B. Monsarrat and C. M. Gosselin, "Workspace analysis and optimal design of a 3-leg 6-DOF parallel platform mechanism," *IEEE Transactions on Robotics and Automation,* vol. 19, no. 6, pp. 954–966, 2004. doi: 10.1109/TRA.2003.819603

[16] X. Zhang *et al.*, "A new composite leaf spring for in-board bogie of new generation high-speed trains," *Applied Composite Materials,* vol. 30, no. 4, pp. 1377–1392, 2023. doi: 10.1007/s10443-022-10095-4

[17] Y. Liu, Y. Zhang, and Q. Xu, "Design and control of a novel compliant constant-force gripper based on buckled fixed-guided beams," *IEEE/ASME Transactions on mechatronics,* vol. 22, no. 1, pp. 476–486, 2016, doi: 10.1109/TMECH.2016.2614966

[18] C. Ott, "Modeling of flexible joint robots," in *Proc. Cartesian Impedance Control of Redundant and Flexible-Joint Robots*: Springer, 2008, pp. 13–27. doi: 10.1007/978-3-540-69255-3_2

[19] J. Knospler, W. Xue, and M. Trkov, "Reconfigurable modular soft robots with modulating stiffness and versatile task capabilities," *Smart Materials and Structures,* vol. 33, no. 6, 065040, 2024. doi: 10.1088/1361-665X/ad4d35

[20] F. Zhao, H. Tang, X. Zou, and X. Li, "A review of optical metrology techniques for advanced manufacturing applications," *Micromachines,* vol. 16, no. 11, 1224, 2025. doi: 10.3390/mi16111224

[21] G. Zhang, S. Yang, P. Hu, and H. Deng, "Advances and prospects of vision-based 3D shape measurement methods," *Machines,* vol. 10, no. 2, 124, 2022. doi: 10.3390/machines10020124

[22] J. Huang, X. Shao, F. Yang, J. Zhu, and X. He, "Measurement method and recent progress of vision-based deflection measurement of bridges: A technical review," *Optical Engineering,* vol. 61, no. 7, 070901, 2022. doi: 10.1117/1.OE.61.7.070901

[23] D. Villalba Rama, M. Gonçalves, J. Dias-de-Oliveira, A. Andrade-Campos, and R. Valente, "IGA-based topology optimization in the design of stress-constrained compliant mechanisms," Structural and Multidisciplinary Optimization, vol. 66, 244, 2023. doi: 10.1007/s00158-023-03697-4

[24] T. Liu and G. Hao, "Design of deployable structures by using bistable compliant mechanisms," *Micromachines,* vol. 13, no. 5, 651, 2022. doi: 10.3390/mi13050651

[25] A. Nowak, L. F. Campanile, and A. Hasse, "An Efficient Modal Approach for Load-Independent Topology Optimization of Compliant Mechanisms," *Structural and Multidisciplinary Optimization,* vol. 68, no. 9, 181, 2025.doi: 10.1007/s00158-025-04058-z

[26] Z. Wan *et al.*, "Flexible Tactile Sensors: Materials, Mechanisms, Structures, and Multifaceted Applications," *Small,* vol. 21, no. 48, e11475, 2025. doi: 10.1002/smll.202511475

[27] P. Tang, "Computational modeling and design of nonlinear mechanical systems and materials," Ph.D. dissertation, Université de Montréal, 2023. doi: 10.71781/9897
[28] A. Klimchik, A. Pashkevich, and D. Chablat, *Stiffness Modeling of Parallel Robots ser. Parallel Robots: Theory and Applications, Springer Nature Switzerland*, 2025, 232. doi: 10.1007/978-3-031-76320-5
[29] M. Ling, X. Zhang, and J. Cao, "Extended dynamic stiffness model for analyzing flexure-hinge mechanisms with lumped compliance," *Journal of Mechanical Design,* vol. 144, no. 1, 013304, 2022. doi: 10.1115/1.4051891
[30] M. Ling, L. Yuan, and X. Zhang, "Static and dynamic compliance analyses of curved-axis flexure hinges: A discrete beam transfer matrix," *Journal of Mechanical Design,* vol. 145, no. 6, 064501, 2023. doi: 10.1115/1.4056757
[31] T. Abhijit and G. Prasanna, "Design and analysis of ultra-precise large range linear motion platforms using compliant mechanism," *IEEE Access,* vol. 10, pp. 94321–94336, 2022. doi: 10.1109/ACCESS.2022.3201343
[32] K.-s. Park and K.-m. Lee, "A Review of Passive Linear Gravity Compensation Mechanisms," *Actuators*, vol. 15, no. 2, 111, 2026. doi: 10.3390/act15020111
[33] M. Warzecha, M. E. Schatz, S. Lucarelli, and C. Jüttner, "Increasing Structural Performance of Space Telescope Mirrors through Simultaneous Shape and Size Optimization," *Aerospace,* vol. 9, no. 11, 646, 2022. doi: 10.3390/aerospace9110646
[34] K.-S. Park and K.-M. Lee, "A review of passive linear gravity compensation mechanisms," *Actuators,* vol. 15, no. 2, 111, 2026. doi: 10.3390/act15020111
[35] S. Seltmann and A. Hasse, "Topology optimization of compliant mechanisms with distributed compliance (hinge-free compliant mechanisms) by using stiffness and adaptive volume constraints instead of stress constraints," *Mechanism and Machine Theory,* vol. 180, 105133, 2023. doi: 10.1016/j.mechmachtheory.2022.105133
[36] A. Humer and S. Platzer, "Efficient Design of Compliant Mechanisms Using Multi-Objective Optimization," arXiv preprint, arXiv:2504.16451, 2025.

Copyright © 2026 by the authors. This is an open access article distributed under the Creative Commons Attribution License which permits unrestricted use, distribution, and reproduction in any medium, provided the original work is properly cited (CC BY 4.0).